Optical Inspection of Material Surface Quality Changes with Laser Displacement Sensors, Including Applications to Laser Inertial Fusion*)

Koichi KASUYA[1,3)], Wardemar MROZ[2)], Boguslaw BUDNER[2)], Shinji MOTOKOSHI[3)], Katsuhiro MIKAMI[4)] and Takayoshi NORIMATSU[4)]

[1)]*Institute of Applied Flow, 3-24-4 Utsukushigaoka-Nishi, Aoba, Yokohama, Kanagawa 225-0001, Japan*
[2)]*Institute of Optoelectronics, MAT, ul. gen. Sylwestra Kaliskiego 2, Warsaw 49, 00-908, Poland*
[3)]*Institute of Laser Technology, c/o ILE Osaka University, 2-6 Yamadaoka, Suita, Osaka 565-0871, Japan*
[4)]*Institute of Laser Engineering, Osaka University, 2-6 Yamadaoka, Suita, Osaka 565-0871, Japan*

(Received 26 May 2012 / Accepted 24 October 2012)

A new method to estimate erosion threshold of various material surfaces with a high-power pulsed electron beam [Appendix] was extended to the surface erosions with various pulsed laser lights. The most interesting result was that the CVD polycrystalline diamond had similar erosion threshold as tungsten. After our extended experiments of this kind in the near future, novel plasma-facing surface materials are expected to be realized for future fusion reactor chambers.

Keywords: material surface erosion, fusion reactor chamber, threshold evaluation, laser created crater, displacement sensor diagnostic, optical grade CVD polycrystalline diamond, universal fusion chamber construction, inner surface monitor

DOI: 10.1585/pfr.8.3404054

1. Introduction

In any system, when an externally generated stimulus exceeds a predetermined threshold value, there is a change in variables related to that system. The specific variable is usually considered to increase from a value that is smaller than the threshold value to one that is larger. The total number of increments required to exceed the threshold value is large. In contrast, when the variable is decreased from a value larger than the threshold value, the total number of decrements in this case is usually much smaller than the number of increments in the above normal case, and this approach is believed to be a more cost effective way of evaluating the threshold value. This is the basis for the method proposed in this article.

A general example of this universal method is shown for the optical inspection of changes in the quality of a material's surface, and example applications are described here. Next, we present some examples of our method that can be extended to a variety of derivatives to investigate not only crater formations but also the optical quality of various optical components such as reflection and/or transmission coefficients under various environmental conditions.

2. Experimental Method and Results

The main material considered in this study is the CVD polycrystalline diamond, particularly the commercial optical grade one. The pulse duration and wavelength of the ArF laser [1] were 10 ns and 190 nm, respectively. The repetition rate and energy per pulse were 5 Hz and 328–358 mJ, respectively. The sample surfaces were irradiated up to 10,000 shots per spot, and the surface erosion profiles were measured using various surface profilers with red laser displacement sensors [2–13].

The diameter and thickness of the diamond sample were 8.0 mm and 0.5 mm, respectively. The samples are normally used as optical windows for various applications. They have broad transparency, high thermal conductivity, and durable and wear resistances; these characteristics are suitable for use in IR and high-power laser optics. Typical craters on a sample after the ArF laser irradiations are shown in Fig. 1 for the cases of 1,000 and 2,000 shots per crator. We can easily observe the laser spot size for these cases in this type of photograph.

The crater profiles were measured with a commercial semiconductor laser displacement sensor combined with a motor-driven precision X–Y stage. They were controlled by a PC, and the three-dimensional profile data were processed by and stored on the same PC. An example of the surface profile results is shown in Fig. 2. Here the upper photograph shows the two-dimensional crater shape, while the daigram in the lower part shows the crater depth as a function of its spot along the central horizontal line of the photograph. The maximum crater depth in this case is ap-

author's e-mail: kasuyakoh@aol.com

*) This article is based on the presentation at the Conference on Inertial Fusion Energy '12.

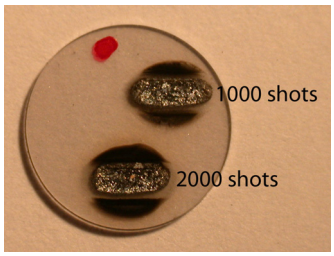

Fig. 1 Typical craters on an optical grade CVD polycrystalline diamond irradiated with an ArF laser.

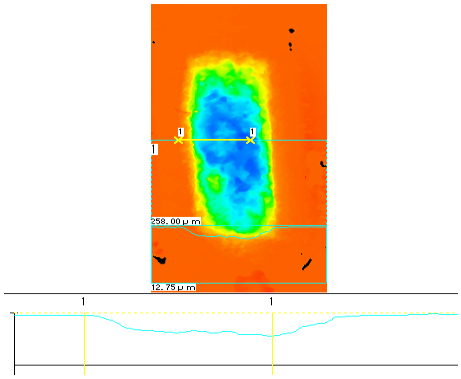

Fig. 2 Three-dimensional analysis of a typical crater with a laser displacement sensor system.

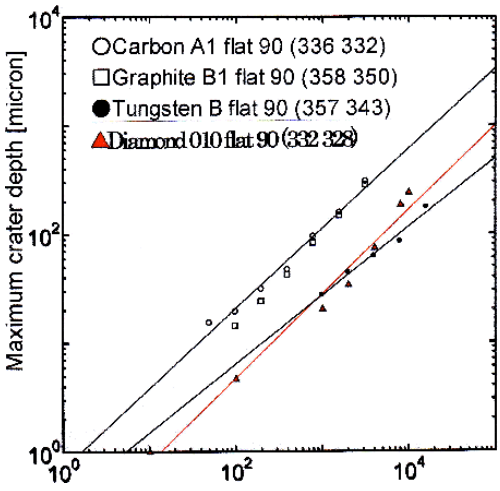

Fig. 3 Maximum crater depth vs. total irradiation number per spot with normal incident ArF laser lights. The cases of C, graphite, W, and diamond are compared.

proximately 48 microns. The total number of laser irradiations per spot were changed from 10 to 100, 1,000, 2,000, 4,000, 8,000, and 10,000.

The threshold shot accumulation numbers required to start the erosions were estimated from the plots of maximum erosion depth vs accumulation numbers in Fig. 3. We compared the erosion threshold of the above-mentioned di-

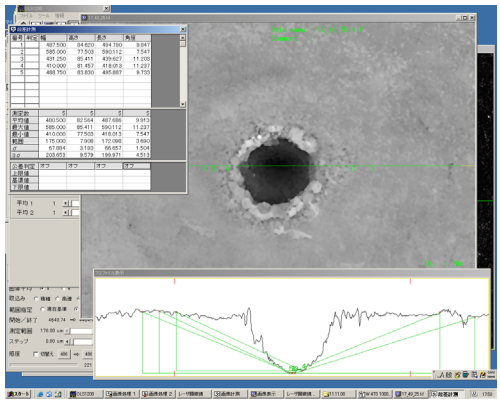

Fig. 4 Laser microscope measurement of tungsten surface eroded with Nd:YAG laser light (initial sample temperature: 473 K, and total laser shot numbers: 4,000).

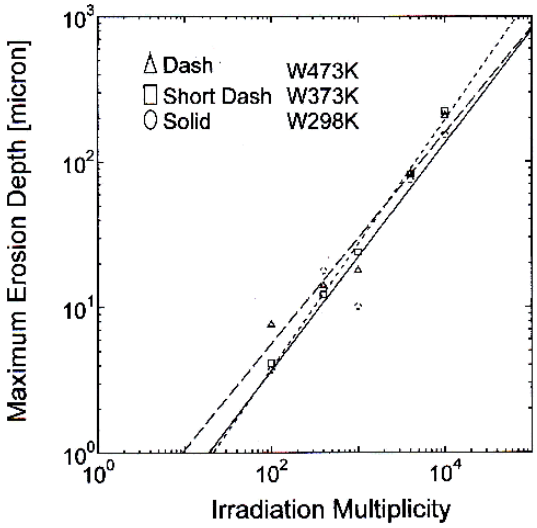

Fig. 5 Erosion of tungsten with initial temperature change, measured with a laser microscope.

amond with that of tungsten. There was a small difference of approximately 10 shots, and the equivalent laser irradiation energy was approximately 3.6-3.9 J, which are attractive properties for such a diamond when used as parts of various structural materials, particularly for the plasma-facing surface materials of nuclear fusion reactors.

In place of the ArF laser lights described above, we used Nd:YAG laser lights (10 ns, 1.06 microns, several mJ/shot, and 10 Hz) to create craters on various material surfaces. An example of three-dimensional crater profiles of tungsten is shown in Fig. 4. In place of the laser displacement sensor system described above, we used a laser microscope for this measurement. The upper part of the photograph shows the X-Y trace of the crater, and the lower part shows the X-Z trace. In addition, we changed the initial temperature before the irradiations from room temperature to 373 K and 473 K. Similar profile measure-

ments were performed with different accumulation numbers of laser irradiations per spot. The final results are shown in Fig. 5, where the maximum erosion depth is plotted as a function of shot accumulation. The parameter is the sample initial temperature before the irradiation. There were not many differences in the erosion depth results as the sample's initial temperature changed within this range.

Different grades of CVD polycrystalline diamonds (thermal management grade and electrochemical grade) were also irradiated with Nd:YAG laser lights. The results are described in additional papers.

3. Applications

Here we explain how the above-mentioned methods with the laser displacement sensors and CVD polycrystalline diamond can be extended for the future development of advanced erosion diagnostic tools.

First, we consider a laser monitor to inspect the surface erosions of the fusion chambers in situ. Although a monitor for the divertor is discussed below, our method is also useful for other parts of MFE chambers (for example, the chamber's first wall) and for the IFE chamber. A cross-sectional diagram of the ITER divertor section is shown in [14]. The inner and outer divertors and a dome are the plasma-facing parts, which receive severe pulsed heat influx under the ELM condition. Examples of the ITER divertor bird-eye views are shown in [15, 16]. Our plan is to inspect these surfaces with our laser monitor and to prevent them from being severely damaged. There are varieties of commercial displacement sensors. In our study, because the object does not move while being inspected, we must instead move the sensor head to observe the object surface. An example from the catalogue (a sensor head section with an optical fiber guide section) is Keyence/Model SI-F10. The spot size of the red semiconductor laser light on the inspected surface changes with the distance between the sensor front head and inspected surface. If the measurable distance from the front head is too short to extend the design of the monitor, different sensors may be selected with a different system design. For the LK-G3000/LK-G500 sensor, a maximum measurable range of 500 (+500, −250) mm with a laser spot size of 0.3 mm is obtained. If we use diamond (either with a partial small area or a relatively large area) on a part of the divertor surface (this is acceptable as long as carbon, graphite, or CFC is used in the existing ITER design), we will be able to place a sensor head behind the divertor plate. In this case, a transparent-type displacement sensor becomes useful in place of a reflection-type sensor. In any case, we must design a complete monitoring system that can fit our object. In the near future, we aim to realize the best-fit design with the best sensor selection. In addition, all of the above-mentioned technical solutions are applicable to not only the divertors but also different types of chamber surfaces, including a very wide range of industrial applications.

It is also possible to realize a laser monitor system to inspect deeper layers under a surface. It is often necessary to carefully inspect such layers because material blisters often occur with a relatively heavy damage underneath the front surface without significantly damaging the front surface. A cursory glance in the fusion chamber will not usually detect the damage to the front surface. Recently, a laser-induced ultrasonic wave diagnostic method is developed for railroad tunnel inspections. We hope that we will be able to convert the same technique to our fusion chamber monitoring system. This will also be one of the focus points of our study in the near future. The latest reports from OMRON Co., Ltd. informed us of a new displacement sensor with a wide-band interferometer-type spectrum light source. This may be useful as a more powerful sensor for our advanced study in the near future.

4. Future Prospects

After obtaining further confirmation of the result shown in Fig. 3 by performing additional experiments and evaluations, we will be able to demonstrate that the polycrystalline CVD diamond can replace conventional plasma-facing surface materials such as CFC and tungsten. It is recommended that a more advanced version of laser displacement sensor is developed with more complex algorithms, and this would enable us to realize an even more favorable diamond material.

Acknowledgments

This work was performed under the joint research project of (1) the Institute of Laser Engineering, Osaka University (under contract number "2011-B2-18") and (2) National Institute of Fusion Science (under contract number "2011-NIFS11KUGK056." The authors acknowledge the support received from the members of the (1) Institute of Laser Engineering, Osaka University, (2) Institute of Laser Technology, (3) Institute of Optoelectronics, MAT, (4) Institute of Applied Flow, and (5) Naka Fusion Institute, Japan Atomic Energy Agency.

Appendix

The first result of our new threshold evaluation method with tungsten irradiation by electron beams is shown in Fig. A1.

Under the electron acceleration voltage and current of 65 kV and 2.28 A, respectively, and under the three types of beam pulse width, the thermal loads on the sample surfaces were a) 1.0 ms: 1,100-1,200 MW/m^2, b) 1.2 ms: 1,400-1,450 MW/m^2, and c) 1.5 ms: 1,460 MW/m^2. The maximum erosion depths of the produced craters were measured using a surface profiler (a combination of a laser displacement sensor, a precision X-Y stage, and their PC controller), and the result is shown in Fig. A1. With the numerical line fitting on the same figure (also with the extrapolation down to the x-axis), we evaluated the threshold pulse

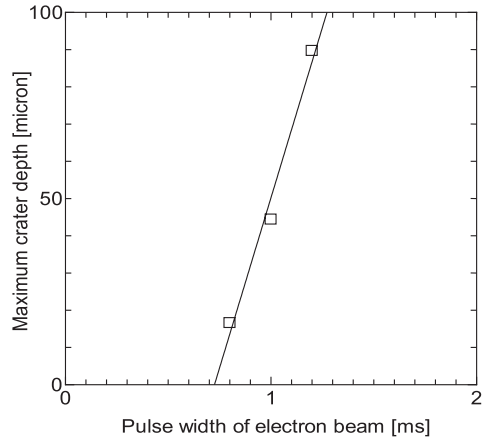

Fig. A1 Erosion threshold evaluation of tungsten irradiated with a single-shot electron beam.

width required to start the surface erosion, from which we could then obtain the threshold thermal load in this case as follows.

The simple estimation equation for the threshold thermal load on the carbon divertor surface with ELM is shown as follows [17].

$$Q/\Delta t^{1/2} = 45\,\mathrm{MJ/m^2/s^{1/2}}, \tag{A.1}$$

where Q is the ELM thermal energy flux [J/m^2] on the divertor surface and Δt is the heat pulse width [s]. Because this equation is only briefly described in the same reference paper, there appears to be no precise derivation process (theoretical or experimental) in other corresponding reference papers. Therefore, we tried to evaluate the exact thermal threshold value from the tungsten case result shown in Fig. A1. The pulse width of the fitting line cross point across the x-axis was approximately 0.73×10^{-3} [s], which we used to calculate the corresponding Q and $\Delta t^{1/2}$. Finally, we found

$$Q/\Delta t^{1/2} = 270\,\mathrm{MJ/m^2/s^{1/2}}. \tag{A.2}$$

Here Q was measured as approximately 1.0 [MJ] using a calorimeter (representative value). A comparison of both Eqs. (A.1) and (A.2) showed that tungsten used in our study was stronger than carbon by approximately 270/45 = 6 factors of magnitude.

[1] K. Kasuya, S. Ozawa, T. Norimatsu, H. Azechi, K. Mima, S. Nakai, S. Suzuki, B. Budner and W. Mroz, 18th Symposium on Gas Flow and Chemical Laser, and High Power Lasers, SPIE Proceedings **7751**, Paper No.12, CD-ROM Distribution (2011).
[2] K. Mima and K. Kasuya, 18th Symposium on Gas Flow and Chemical Lasers, and High Power Lasers, SPIE Proceedings **7751**, Paper No.52, CD-ROM Distribution (2011).
[3] K. Kasuya *et al.*, 19th Meeting of ITPA Topical Group on Diagnostics, URL-Record, in print (2011).
[4] K. Kasuya, S. Ozawa, T. Norimatsu, H. Azechi, K. Mima, S. Nakai, S. Suzuki, B. Budner and W. Mroz, Fusion energy conference 2010 IFE satellite meeting 1 (2010).
[5] K. Kasuya *et al.*, 5th IAEA Technical Meeting on Physics and Technology of Inertial Fusion Energy, in print (2010).
[6] K. Kasuya *et al.*, Research Coordinated Meeting of IAEA Coordinated Research Project on Pathways to Energy from IFE (Inertial Fusion Energy) -An Integrated Approach, in print (2010).
[7] K. Kasuya *et al.*, Proceedings of 4th IAEA Technical Meeting on Physics and Technology of IFE Targets and Chambers, CD-ROM Distribution (2008).
[8] K. Kasuya *et al.*, Proceedings of the 1st IAEA Coordinated Meeting of the Coordinated Research Project on Pathways to Energy from IFE (Inertial Fusion Energy) -An Integrated Approach, IAEA Report, CD-ROM Distribution (2007).
[9] K. Kasuya *et al.*, 22nd IEEE/NPSS Symposium on Fusion Engineering, CD-ROM Distribution (2007).
[10] K. Kasuya *et al.*, Proceedings of the Japan-US Workshop on Heat Removal and Plasma Materials Interactions for Fusion, Fusion High Power Density Components and System, and IEA Workshop on Solid Surface Plasma Facing Components, URL-Record (2007).
[11] K. Kasuya *et al.*, Fusion Eng. Des. **81**, 8-14, 1653 (2006).
[12] K. Kasuya *et al.*, Proceedings of SPIE International Congress on Optics and Optoelectronics, Conference on Laser and Application, SPIE Proceedings **5958** [1T], 1 (2005).
[13] K. Kasuya *et al.*, J. Nucl. Mater. **235**, 313 (2002).
[14] N. Asakura *et al.*, 34th EPS Conference on Plasma Phys. ECA **31F**, P-1.051 (2007).
[15] K. Ezato, S. Suzuki, Y. Seki, K. Yokoyama, M. Enoeda, M. Akiba, S. Mori, S. Satoh, S. Merola and M. Pick, Proc. of the 22nd IAEA Fusion Energy Conference, IT/P7-17, CD-ROM distribution (2010).
[16] S. Suzuki, J. Plasma Fusion Res. **87**, 607 (2011) [in Japanese]. http://www.jspf.or.jp/Journal/PDF_JSPF/jspf2011_09/jspf2011_09-607.pdf
[17] A. Leonard *et al.*, 1998 ICPP and 25th EPS Conference on Controlled Nuclear Fusion and Plasma Physics, ECA **22C**, 679 (1998).